

Deep Robust Single Image Depth Estimation Neural Network Using Scene Understanding

Haoyu Ren, Mostafa El-khamy, Jungwon Lee
SOC R&D, Samsung Semiconductor Inc.
9868 Scranton Road, San Diego, CA, US

{haoyu.ren, mostafa.e, jungwon2.lee}@samsung.com

Abstract

Single image depth estimation (SIDE) plays a crucial role in 3D computer vision. In this paper, we propose a two-stage robust SIDE framework that can perform blind SIDE for both indoor and outdoor scenes. At the first stage, the scene understanding module will categorize the RGB image into different depth-ranges. We introduce two different scene understanding modules based on scene classification and coarse depth estimation respectively. At the second stage, SIDE networks trained by the images of specific depth-range are applied to obtain an accurate depth map. In order to improve the accuracy, we further design a multi-task encoding-decoding SIDE network DS-SIDENet based on depthwise separable convolutions. DS-SIDENet is optimized to minimize both depth classification and depth regression losses. This improves the accuracy compared to a single-task SIDE network. Experimental results demonstrate that training DS-SIDENet on an individual dataset such as NYU achieves competitive performance to the state-of-art methods with much better efficiency. Ours proposed robust SIDE framework also shows good performance for the ScanNet indoor images and KITTI outdoor images simultaneously. It achieves the top performance compared to the Robust Vision Challenge (ROB) 2018 submissions.

1. Introduction

Single image depth estimation (SIDE) is a key feature of understanding the geometric structure of the scene. In particular, the depth map can be used to infer the 3D structure, which is the basic element of many topics in 3D vision, such as image reconstruction, image rendering, and shallow depth of the field. SIDE is an ill-posed problem since a single 2D image may be produced from an infinite number of distinct 3D scenes. To overcome this ambiguity, typical methods focus on exploiting statistically meaningful features, such as perspective and texture information,

object locations, and occlusions. Recently, with the prosperity of deep convolutional neural networks (CNNs), many deep learning-based methods have achieved significant performance improvement.

This work aims to address two main issues of deep CNNs for SIDE. Most of current SIDE methods train different networks for individual datasets, which makes models be specific to certain domains. As a result, the large differences between different datasets such as indoor and outdoor patterns limit the generalization ability of the SIDE network. A model achieving considerable performance on one dataset will perform poorly on the other one. Hence, the first issue we aim to address is how to design a framework for blind SIDE, where both indoor images and outdoor images are fed into same SIDE network. Existing SIDE networks utilize very deep architecture such as ResNet-101 [10] or ResNext-101 [20] as backbone. The sizes of these networks are very large. In addition, some of existing SIDE networks such as DORN [10] contain fully connected layers. So a sliding-window strategy is required during the prediction to make the testing image size same as training. As a result, the efficiency and flexibility of such networks is not very good. Hence, the second issue we aim to address is designing an efficient fully-convolutional SIDE network achieving high accuracy as well.

In this paper, we propose an effective two-stage framework for robust single image depth estimation, as shown in Fig. 1. Our framework starts by a scene understanding module, where the input RGB image is categorized into low depth-range or high depth-range. Then we apply different SIDE networks trained by low depth-range RGB images and high depth-range images respectively, to estimate an accurate depth map. Since we do not have any prior knowledge before the testing, our framework is blind SIDE. We show that the scene understanding module can be implemented by either a scene classification network, or a coarse single image depth estimation network. Both of them work well for the robust SIDE task of Robust Vision Challenge (ROB) 2018 [1], where the testing images are randomly

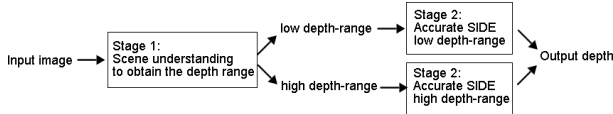


Figure 1. Our proposed two-stage robust SIDE framework.

sampled from ScanNet [6] and KITTI[11] datasets.

Next, we present an efficient fully-convolutional neural network DS-SIDENet for single image depth estimation. DS-SIDENet is a multi-task network following the encoding-decoding architecture [17]. The encoding part consists of several depthwise separable (DS) convolutional layers to extract discriminative features from the input image. The decoding part consists of two branches corresponding to the depth classification task and the depth regression task. In the depth classification branch, the network generates pixel-wise classification labels of the quantized depth. In the depth regression branch, a continuous depth map is directly estimated. During the training, we optimize the loss functions considering these two branches at the same time, while only the depth classification result is utilized during the predication. This improves the discriminative ability of the network, without adding computational cost during depth estimation. Our multi-task network is different from existing multi-task networks [8] which considers depth estimation and semantic segmentation together. The two tasks in DS-SIDENet can be considered as different formulations of same depth estimation problem, instead of different problems in [8]. We show that DS-SIDENet can achieve better performance than existing SIDE networks in NYU-Depth-v2 [9] dataset. Our proposed robust SIDE based on DS-SIDENet achieves the 1st rank compared to ROB 2018 submissions.

The contributions of our work can be summarized as:

- We propose a two-stage framework effective for robust SIDE based on scene understanding. Two different scene understanding modules, scene classification and coarse depth estimation, are discussed
- We design an efficient SIDE network based on depthwise separable convolution. It achieves considerable accuracy and efficiency concurrently
- We show that doing multi-task learning in SIDE by considering depth classification and depth regression together is helpful to improve the overall accuracy

2. Related work

Previous approaches for depth estimation from single images can be categorized into two main groups, methods operating on hand-crafted features, and methods adopting deep neural networks. Earlier works addressing the depth estimation task belong to the first category. Hoiem et al. [12] introduced photo pop-up, a fully automatic method for

creating a basic 3D model from a single photograph. Karsch et al. [13] developed Depth Transfer, a non-parametric approach where the depth of an input image is reconstructed by transferring the depth of multiple similar images with warping and optimizing procedures. Ladicky [16] demonstrated the benefit of combining semantic object labels with depth features. Saxena et al. [25] introduced a multi-scale conditional random field (CRF) to extract multi-scale context information for depth estimation.

More recent approaches for depth estimation are based on convolutional neural networks. In the pioneer work [9], Eigen et al. introduced a coarse-to-fine network, and utilized the scale-invariant loss to improve the accuracy of the estimated depth map. This work is further extended in [8], where the depth estimation, surface normal estimation, and semantic segmentation are integrated into one unified network. Li et al. [19] considered a loss function with components in both the depth domain and the gradient of depth domain. Fu. et al. [10] introduced a spacing-increasing discretization strategy to discretize depth and re-casted depth network learning as an ordinal regression problem. Their method achieves significant accuracy improvement compared to previous methods.

Most of above works use some backbones with fully connected layer. This will increase the model complexity and computation cost. In addition, the input image size is restricted during the testing. To solve this problem, a fully convolutional network was proposed by Laina et al. [17]. A revised version of this work is introduced in [21], where randomly sampled sparse depth is adopted together with the RGB image to predict a dense depth map. Chen et al. [4] used a fully-convolutional network to predict the relative depth map, e.g., a relationship between the depths of any two pixels. Kuznetsov et al. [15] utilized semi-supervised learning for SIDE, where supervised learning on sparse measurements is complemented with unsupervised learning of the left-right consistency in stereo images. Cheng et al. [5] proposed a spatial propagation network to learn the affinity matrix and showed its effectiveness to improve the performance of existing SIDE networks. All of the above CNNs are constructed based on some computationally expensive architecture. In contrast, our DS-SIDENet is constructed by depthwise separable convolution [23], which is more efficient during the prediction.

3. Robust single image depth estimation

Blind depth estimation is very important in real scenario. A good SIDE system should consequently perform well on a variety of datasets with different characteristics, e.g., for both the indoor scenario and the outdoor scenario. One straightforward solution is to mix the training data of indoor and outdoor images to train one network, which is utilized by many of the ROB submissions. For example, Li et al.

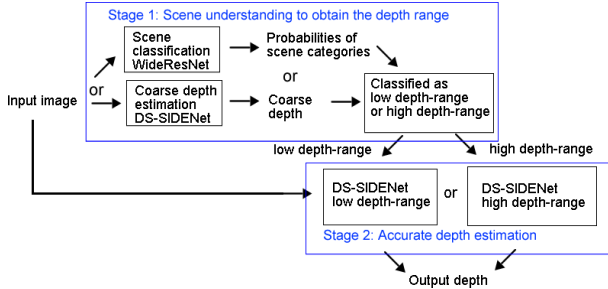


Figure 2. Robust SIDE based on two different scene understanding modules.

[20] resized the KITTI and ScanNet images to 320×256 , and utilized a channel-wise attention mechanism to adaptively select the discriminative channels of features for indoor and outdoor scenarios. But this will decrease the accuracy compared to training different networks for different datasets.

The major difficulty of blind SIDE is the contextual difference between scenes. Different scene types tend to have different depth-ranges. For example, outdoor scenes tend to have a larger depth-range than indoor scenes. So we propose to use scene understanding to capture the depth-range, in order to support the following depth estimation. We introduce a two-stage framework as illustrated in Fig. 2. The first stage is a scene understanding module, which classifies the input RGB image into low depth-range category (all objects are close to camera) or high depth-range category (including objects far away, e.g., distance higher than threshold). Then we apply different SIDE networks for the low depth-range images and high depth-range images respectively to get an accurate depth map. In this section, we give two different solutions for the scene understanding stage.

Our first solution is using the scene classification methods to get the probability of the scenes, and obtaining the depth-range from these probabilities. Assume we have scene categories with ‘low depth-range’ or ‘high depth-range’ labels based on their context, given the estimated probabilities of these scenes from a scene classification network, the depth-range can be calculated by a ‘majority voting’ from the top- K scenes with highest probability. For example, the input image is classified as ‘low depth-range’ if there are more than $K/2$ ‘low depth-range’ votes from the top- K scene categories. Other methods can also be used to decide the depth-range such as weighted voting, or the expected depth-range based on the predicted scene probabilities and the average depth-range of each scene. In this paper, we show that even the simple majority voting strategy is good in the ROB challenge. In our implementation, we use the WideResNet-18 trained on the Places-365 dataset [27] as the scene classification network. This dataset consists of 365 labeled scene categories, such as sky, arena, iceberg, etc. Given an input image, we use the top-15 ($K = 15$)

predicted scene categories to vote for depth-range.

Our second solution is training a coarse depth estimation network by mixing images from different depth-ranges together. Then the depth-range can be inferred from the statistics of the estimated coarse depth map. We calculate the maximum depth d_{max} of the whole estimated depth map, and compare it to a threshold σ . If $d_{max} > \sigma$, the RGB input is categorized as of high depth-range, otherwise it will be categorized as of low depth-range. To decide σ , we calculate the maximum estimated depth statistic using the validation images of the ROB 2018 challenge [1], from which we select σ as 5.89. In our implementation, the coarse depth-range estimation network has the same architecture as that of the low depth-range DS-SIDENet given in Table 1 and Table 2.

After obtaining the depth-range, we apply one of the two DS-SIDENets optimized for the low depth-range images and high depth-range images to generate an accurate depth map. We also investigated the ‘coarse-to-fine’ architecture proposed in [9][21], by utilizing an RGBD network which takes the estimated depth from the coarse depth estimation as an additional feature with the RGB channels. However, due to the inaccurate depth estimates from the coarse network, no significant performance gain was observed. It will be difficult for RGBD depth refinement with an inaccurate sparse depth features.

4. DS-SIDENet

We propose a single image depth estimation network DS-SIDENet based on depthwise separable convolutions and encoder-decoder architecture [17]. As shown in Fig. 3, our network consists of two parts, the encoding part, and a two-branch decoding part.

4.1. Encoding

The encoding part contains several depthwise separable convolutional layers [23] to extract the discriminative features from the input image, as given in Table 1. Each depthwise separable convolutional layer consists of a depthwise convolutional layer and a point-wise convolutional layers. The low depth-range images have different characteristics with the high depth-range images, e.g., indoor and outdoor images have different context. The encoding part of low depth-range network (e.g., trained in NYU) is slightly different from the high depth-range network (e.g., trained in KITTI). We downsample the output feature map size of the high depth-range encoding module by $\times 4$, and the low depth-range encoding module by $\times 32$.

4.2. Decoding

Since the output feature maps of the encoding part are downsampled, the decoding part requires several upsampling modules to retrieve the input feature map size. A base-

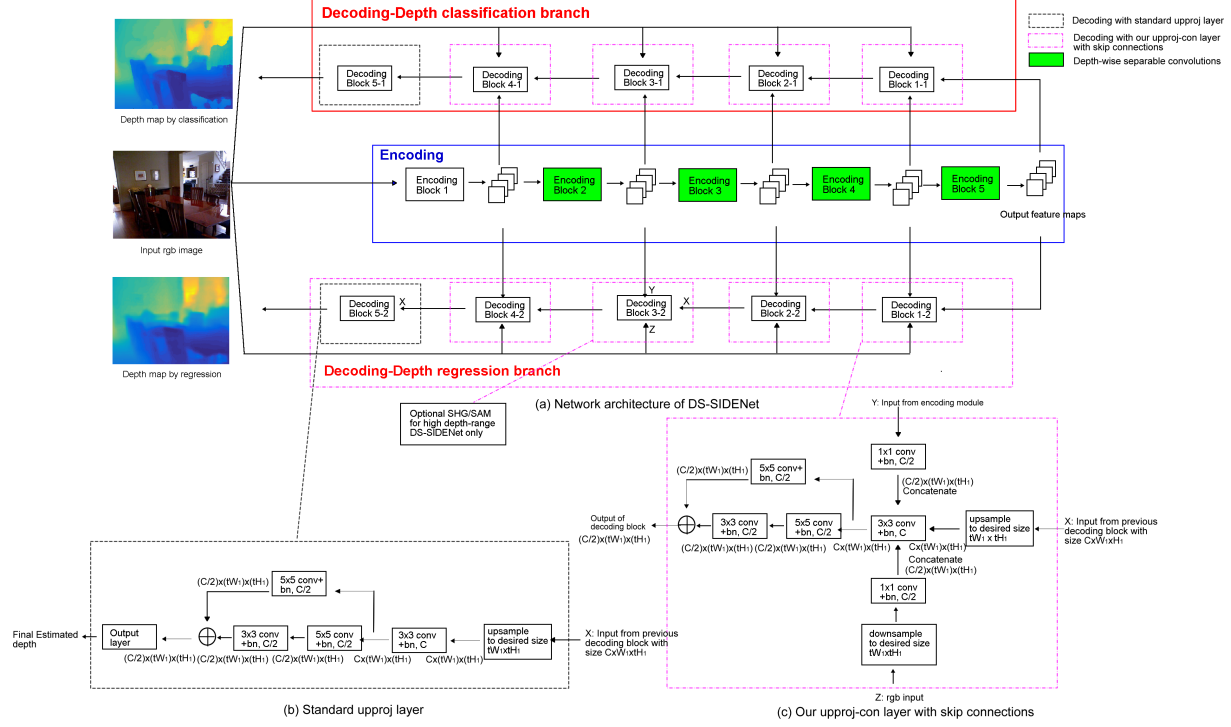


Figure 3. (a) Network architecture of DS-SIDENet. (b) The standard upproj layer in [17]. The ‘output layer’ in classification branch is different from the one in regression branch. (c) Our upproj-con layer with skip connections. The ‘X’, ‘Y’ and ‘Z’ correspond to the three input feature maps of this block. ‘t’ is the scale difference between the input feature map and output feature map. ‘ $C \times W_1 \times H_1$ ’ is the size of input feature maps of the decoding block.

Table 1. Network architecture of the encoding part of DS-SIDENet. The ‘Block1’ to ‘Block5’ correspond to the encoding blocks displayed in Fig. 3(a). ‘s’ means stride, ‘d’ means dilation rate, ‘dw’ means depthwise separable convolutions. ‘convbn’ layer includes a convolutional layer, followed by a batch normalization layer.

layer	low depth-range network		high depth-range network	
	layer setting	output dimension	layer setting	output dimension
input		$3 \times W \times H$		$3 \times W \times H$
Block 1	$convbn, 3 \times 3, 32, s2, d1$ $convbn, 3 \times 3, 64, s1, d1$	$64 \times \frac{1}{2}W \times \frac{1}{2}H$	$convbn, 3 \times 3, 32, s2, d1$ $convbn, 3 \times 3, 64, s1, d1$	$64 \times \frac{1}{2}W \times \frac{1}{2}H$
Block 2	$[convbn, 3 \times 3, 64, s1, d1, dw] \times 3$ $convbn, 3 \times 3, 128, s2, d1, dw$	$128 \times \frac{1}{4}W \times \frac{1}{4}H$	$[convbn, 3 \times 3, 64, s1, d1, dw] \times 3$ $convbn, 3 \times 3, 128, s2, d1, dw$	$128 \times \frac{1}{4}W \times \frac{1}{4}H$
Block 3	$[convbn, 3 \times 3, 128, s1, d1, dw] \times 3$ $convbn, 3 \times 3, 256, s2, d1, dw$	$256 \times \frac{1}{8}W \times \frac{1}{8}H$	$[convbn, 3 \times 3, 128, s1, d1, dw] \times 3$ $convbn, 3 \times 3, 256, s1, d1, dw$	$256 \times \frac{1}{4}W \times \frac{1}{4}H$
Block 4	$[convbn, 3 \times 3, 32, s1, d2, dw] \times 12$ $convbn, 3 \times 3, 256, s2, d1, dw$	$256 \times \frac{1}{16}W \times \frac{1}{16}H$	$[convbn, 3 \times 3, 32, s1, d2, dw] \times 12$ $convbn, 3 \times 3, 256, s1, d1, dw$	$256 \times \frac{1}{4}W \times \frac{1}{4}H$
Block 5	$convbn, 3 \times 3, 256, s2, d1, dw$ $convbn, 1 \times 1, 512, s1, d1$	$512 \times \frac{1}{32}W \times \frac{1}{32}H$	$convbn, 3 \times 3, 256, s1, d1, dw$ $convbn, 1 \times 1, 128, s1, d1$	$128 \times \frac{1}{4}W \times \frac{1}{4}H$

line solution is the ‘upproj’ layer proposed in [17], as given in Fig. 3(b), which achieves better performance compared to upsampling by simple deconvolution layer. Inspired by the U-Net architecture [24], we design an improved upsampling layer with additional skip connections from the encoding part and RGB input, denoted as ‘upproj-con’ layer. As shown in Fig. 3(c), assume the input feature map size from the previous decoding layer is $C \times W_1 \times H_1$, the output feature map size of ‘upproj-con’ layer will be $\frac{C}{2} \times tW_1 \times tH_1$, where t is the scale difference between the input feature map and output feature map.

The decoding part consists of two branches, the depth classification branch and the depth regression branch. These two branches have mostly the same network architecture, but they are optimized with different loss functions. Each of these two branches consists of several ‘upproj-con’ decoding blocks and one additional ‘upproj’ block placed before obtaining the final depth output, as given in Fig. 3(a) and Table 2. For the low depth-range network, we set all $t = 2$. For the high depth-range network, we set some of these t to 1 since the output of the encoding part of high depth-range network is only downsampled 4 times. In ad-

dition, we replace the third upsampling module by stacked network modules such as stacked hourglass (SHG) since it shows superior performance in the outdoor disparity estimation task [3]. We further adopt the stacked atrous multi-scale (SAM) module proposed in [7] instead of standard SHG, which replaces the downsampling and upsampling in SHG by atrous convolutions. An ablation study of using different decoding blocks is given in section 5.3.2.

4.3. Multi-task loss function

In the classification branch, the network performs depth classification after quantizing the continuous depth into several bins. We follow the quantization scheme proposed in DORN [10], where depth-range $[\alpha, \beta]$ is uniformly quantized into K bins in the log scale. As shown in Eq. 1, the input continuous depth x is quantized to discrete value b , K is the number of bins, and q is the width of each bin.

$$\begin{aligned} b &= \text{round}(\log_{10}(x) - \log_{10}(\alpha))/q \\ q &= (\log_{10}(\beta) - \log_{10}(\alpha))/K \end{aligned} \quad (1)$$

When calculating the loss function of the classification branch, we use a soft classification loss similar to disparity estimation [3], where the expected depth is the weighted sum of the quantized depth probabilities and the quantized depth values, and is the predicted depth for each pixel location. Let p_i^j represents the probability of pixel i being quantized depth j , and D is the maximum quantized depth b_{max} in Eq. 1 when $x = \beta$, the expected quantized depth d_i of pixel i is calculated as $d_i = \sum_{j=1}^D j \times p_i^j$. A smooth L_1 loss is utilized to measure the difference $y = d_i - d_{i,qt}^*$ between the predicted quantized depth d_i and the ground truth quantized depth $d_{i,qt}^*$, as given in Eq. 2.

$$\text{smooth}_{L_1}(y) = \begin{cases} 0.5y^2 & \text{if } |y| < 1 \\ |y| - 0.5 & \text{otherwise} \end{cases} \quad (2)$$

In the regression branch, the network directly regresses the output feature maps to a continuous disparity map. We use the L_1 loss between the output and ground-truth depth to measure the regression accuracy. Both the classification branch and the regression branch are optimized simultaneously using multi-task learning, where the final loss function L is a linear combination of the above two loss functions, as shown in Eq. 3, where $d_{i,qt}^*$ is the quantized depth ground truth, and d_i^* is the continuous depth ground truth. The weights w_1 and w_2 are set to 1 empirically.

$$L = \sum_i w_1 \cdot \text{smooth}_{L_1}(d_{cls,i}, d_{i,qt}^*) + w_2 \cdot L_1(d_{reg,i}, d_i^*). \quad (3)$$

In section 5.3.1, we show that the depth maps from either the classification branch or the regression branch of DS-SIDENet is better than the outputs from the single task

SIDE network. We also observe that the classification output is more accurate than regression output. We only use the classification output during the testing, so that the computational cost will not increase.

5. Experiments

5.1. Datasets and network training

We first utilize NYU dataset to show the effectiveness of the proposed DS-SIDENet. The NYU-Depth-v2 [9] dataset consists of RGB and depth images collected from 464 different indoor scenes. We use the official split of data as [9], where 249 scenes are used for training and the rest 215 for testing. Since all NYU images are indoor images with relatively small depth, we train a low depth-range DS-SIDENet on this dataset.

Next, we follow the robust single image depth estimation challenge in ROB 2018 [1], where the same depth estimation system is evaluated on both the ScanNet indoor images and the KITTI street-view images. The ScanNet [6] is a large-scale RGB-D dataset for indoor scene reconstruction, which contains 2.5 million RGB images in 1,513 scenes. Original RGB images are captured at a resolution of 1296×968 and depth at 640×480 . The KITTI single image depth prediction dataset [11] is a real-world dataset with street views from a driving car. It contains about 46,000 training stereo image pairs with sparse ground-truth depth. KITTI image size is around 1240×370 . We use the official ROB training/validation/testing split for these two datasets.

Our robust SIDE framework consists of three modules, the scene understanding, low depth-range DS-SIDENet, and high depth-range DS-SIDENet. We resize ScanNet images to 320×240 to train the low depth-range DS-SIDENet, and zero pad KITTI images to 1248×384 to train the high depth-range DS-SIDENet. As mentioned in Section 3, the scene understanding can be achieved by either a scene classification network, or a coarse depth estimation network. For scene classification, we utilize the official model of WideResNet-18 trained on the Places-365 dataset, and resize the input RGB image to 224×224 during the testing to predict the scene probabilities. For coarse depth estimation, we mix the training images from ScanNet and KITTI to train a DS-SIDENet. The ScanNet training images are downsampled to 320×240 . The KITTI training images are zero padded to 1248×384 and downsampled to 832×256 . Then random 320×240 patches are cropped to keep the same size as ScanNet.

We utilize multiple evaluation metrics to evaluate the performance of DS-SIDENet, including mean relative absolute error (REL), mean relative squared error (sqREL), root mean square error (RMSE), inverse root mean square error (iRMSE), scale invariant logarithmic error (SIlog), mean average error (MAE), and δ threshold ($\delta_i = \delta < 1.25^i$).

Table 2. Network architecture of each of the decoding branch in DS-SIDENet. ‘Block i’ corresponds to the ‘Decoding block i-1’ and ‘Decoding block i-2’ in Fig. 3(a), $i=1,2,\dots,5$. ‘SAM’ has exact same architecture as the one in [7], where 3 AM modules are stacked.

layer	low depth-range network		high depth-range network	
	layer setting	output dimension	layer setting	output dimension
Input feature maps		$512 \times \frac{1}{32} W \times \frac{1}{32} H$		$128 \times \frac{1}{4} W \times \frac{1}{4} H$
Block 1	upproj-con, $t = 2$	$256 \times \frac{1}{16} W \times \frac{1}{16} H$	upproj-con, $t = 1$	$64 \times \frac{1}{4} W \times \frac{1}{4} H$
Block 2	upproj-con, $t = 2$	$128 \times \frac{1}{8} W \times \frac{1}{8} H$	upproj-con, $t = 1$	$32 \times \frac{1}{4} W \times \frac{1}{4} H$
Block 3	upproj-con, $t = 2$	$64 \times \frac{1}{4} W \times \frac{1}{4} H$	SAM	$32 \times \frac{1}{4} W \times \frac{1}{4} H$
Block 4	upproj-con, $t = 2$	$32 \times \frac{1}{2} W \times \frac{1}{2} H$	upproj-con, $t = 2$	$16 \times \frac{1}{2} W \times \frac{1}{2} H$
Block 5	upproj, $t = 2$	$1 \times W \times H$	upproj, $t = 2$	$1 \times W \times H$

Table 3. Depth estimation accuracy of different SIDE networks in NYU dataset.

Method	REL	RMSE	δ_1	δ_2	δ_3
Eigen [8]	0.158	0.641	0.769	0.950	0.988
Chakrabarti [2]	0.149	0.620	0.806	0.950	0.988
Laina [17]	0.127	0.573	0.629	0.899	0.971
Li [19]	0.152	0.611	0.789	0.955	0.988
MS-CRF [26]	0.121	0.586	0.811	0.954	0.987
DORN [10]	0.115	0.509	0.828	0.965	0.992
DS-SIDENet	0.113	0.501	0.833	0.968	0.993

More details can be found in [9][5].

5.2. Comparison to existing methods

First we use the NYU dataset to evaluate our DS-SIDENet. In Table 3, we give the comparison of our DS-SIDENet to some commonly-used SIDE methods. It can be seen that our DS-SIDENet achieves better accuracy than the state-of-art SIDE method DORN [10]. In addition, our DS-SIDENet takes only 150ms to predict a 640×480 image in single Tesla V100 GPU, which is much faster than 600 ms of DORN, and 1 second of MS-CRF. This signifies the advantage of depthwise separable convolutions. Some example outputs are given in Fig. 4, where better estimated depth maps are generated by DS-SIDENet.

Next, we show the accuracy of our robust SIDE framework in ScanNet and KITTI, in Table 4 and Table 5 respectively. The scene understanding is achieved by WideResNet scene classification in ‘Ours-sc’, and by DS-SIDENet coarse depth estimation in ‘Ours-cde’. It can be seen that we achieve best accuracy in both the ScanNet and KITTI datasets, compared to top ROB submissions¹. We also notice that the SIDE accuracy using scene classification is exactly the same as the one using coarse depth estimation. The reason is that both of these two methods are able to achieve 100% classification accuracy in the ROB test set when classifying ScanNet images to low depth-range, and classifying KITTI images to high depth-range. This gives us another advantage that our robust SIDE framework will

¹The ScanNet leaderboard is not updated anymore. For KITTI leaderboard, please see the our DS-SIDENet-ROB submission in http://www.cvlibs.net/datasets/kitti/eval_depth.php?benchmark=depth_prediction, ROB submissions have ‘ROB’ in their name.

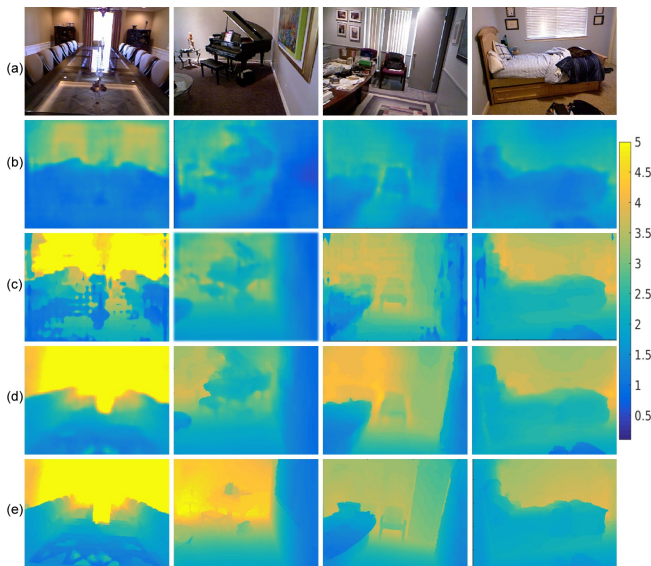


Figure 4. Example outputs of DS-SIDENet in NYU dataset, as well as state-of-art SIDE methods. (a) RGB input (b) Laina [17] (c) DORN [10] (d) Ours DS-SIDENet (e) Ground-truth.

not decrease the accuracy much compared to training different SIDE networks for different datasets. In Section 5.3.3, we show that the accuracy of using coarse depth estimation is sensitive to the threshold of depth-range. In realistic scenario, using scene classification will be better since it provides an independent voting into the scene types and will be less sensitive to threshold errors. We also notice that if we directly use the coarse depth as the final output (‘cde only’), the accuracy is much worse. This signifies the advantage of our robust SIDE framework, compared to training one network based on dataset fusion. Due to the high-efficiency of DS-SIDENet, our robust SIDE network still takes 300-400ms on average to process the ROB testing images in single Tesla V100 GPU. Some example outputs of KITTI images are given in Fig. 5.

As summary, our DS-SIDENet is effective for single image depth estimation. Our robust SIDE framework based on DS-SIDENet is capable of providing considerable depth estimation results for both indoor and outdoor scenarios.

Table 4. Depth estimation accuracy in ScanNet test set, compared to the ROB submissions. ‘cde’ means coarse depth estimation, ‘sc’ means scene classification.

Method	RMSE	MAE	REL	sqREL
CSWS-ROB [18]	0.31	0.24	0.15	0.06
DABC-ROB [20]	0.29	0.22	0.14	0.06
DORN-ROB [10]	0.29	0.22	0.14	0.06
cde only	0.366	0.292	0.191	0.113
Ours-sc	0.287	0.219	0.138	0.057
Ours-cde	0.287	0.219	0.138	0.057

Table 5. Depth estimation accuracy in KITTI test set, compared to ROB submissions. ‘cde’ means coarse depth estimation, ‘sc’ means scene classification.

Method	iRMSE	REL (%)	Sillog	sqREL (%)
DABC-ROB [20]	15.53	12.72	14.49	4.08
DORN-ROB [10]	15.96	10.35	13.53	3.06
CSWS-ROB [18]	16.38	11.84	14.85	3.48
cde only	19.96	20.17	21.22	6.75
Ours-sc	14.61	10.08	12.88	2.78
Ours-cde	14.61	10.08	12.88	2.78

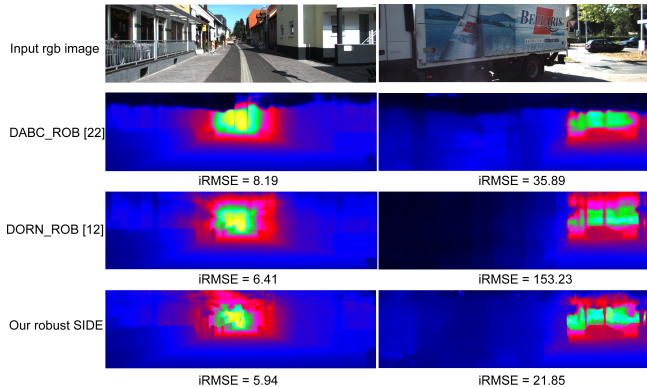


Figure 5. Example outputs of our robust SIDE framework in KITTI SIDE test set, comparison to ROB submissions.

5.3. Ablation study and discussions

In this section, we give ablation study of the key modules of our DS-SIDENet and robust SIDE framework.

5.3.1 Multi-task vs. single-task in DS-SIDENet

First, we test DS-SIDENets with different tasks in depth estimation, which corresponds to different decoding branches. We consider three different branches, including the standard depth classification with cross-entropy loss (hard-cls), the standard depth regression (reg), and the soft classification loss (soft-cls) in DS-SIDENet. In Table 6, we train DS-SIDENets for the above three tasks, as well as our multi-task two-branch network which combines them. It can be seen that the DS-SIDENet based on ‘soft-cls’ loss achieves the best performance among the single-task networks. This observation is consistent to the one in disparity estimation

Table 6. Accuracy comparison of DS-SIDENets with different tasks. RMSE and REL in NYU dataset are given.

Method	REL	RMSE	Training	Testing
DS-SIDENet	0.122	0.518	reg	reg
DS-SIDENet	0.137	0.522	hard-cls	hard-cls
DS-SIDENet	0.120	0.511	soft-cls	soft-cls
DS-SIDENet	0.126	0.514	hard-cls+reg	hard-cls
DS-SIDENet	0.119	0.515	hard-cls+reg	reg
DS-SIDENet	0.113	0.501	soft-cls+reg	soft-cls
DS-SIDENet	0.117	0.510	soft-cls+reg	reg



Figure 6. Example output of two branches from DS-SIDENet.

[14], where the cross-entropy loss performs worse compared to the one based on soft-probability. In addition, we notice that the multi-task networks clearly show better performance than the single-task networks. This can be explained as the multi-task learning is able to improve the discriminative ability and generalization power of the encoding module.

In Fig. 6, we visualize the outputs of reg and soft-cls branches of our DS-SIDENet. It can be seen that comparing to the regression branch, the output of the classification branch is sharper. These two branches reflect different characteristics. This motivates us to further train a fusion network [22] over the outputs of these two branches. Our preliminary results show that the accuracy can be further enhanced by adding such fusion module.

5.3.2 Using different decoding layers in DS-SIDENet

Next, we compare the DS-SIDENets using different decoding layers. In Table 7, we give the comparison between our decoding layer ‘upproj-con’ (row 5) and the standard ‘upproj’ layer (row 2), as well as with and w/o skip connections (row 3/4). It can be seen that the DS-SIDENet with our ‘upproj-con’ layers shows superior performance than others in NYU dataset. If we remove either the skip connection from the encoding part, or the skip connection from the RGB input, the accuracy will decrease. The reason is that the skip connection of the encoding part includes some high-level information, and the skip connection of the RGB input is similar to a pooling layer which captures global context. Integrating these information into the decoding process will be helpful.

In Table 8, we give the accuracy of the high depth-range DS-SIDENets in KITTI validation dataset, with and w/o SHG/SAM in the decoding part. It can be seen that the ac-

Table 7. Comparison of different decoding layers in DS-SIDENet. RMSE and REL in NYU dataset are given.

Method	REL	RMSE	Skip-encoding	Skip-RGB
DS-SIDENet	0.126	0.556	no	no
DS-SIDENet	0.119	0.527	yes	no
DS-SIDENet	0.121	0.532	no	yes
DS-SIDENet	0.113	0.501	yes	yes

accuracy of DS-SIDENet with SAM decoding module is better than the one with SHG decoding module, and also better than without either SHG or SAM modules. A potential reason is that the stacked hourglass provides larger receptive field as well as keeping a relatively larger feature map size, which is more important for the high depth-range images in outdoor scenarios. With carefully designed dilated convolutions, SAM can aggregate denser features while avoiding downsampling operations in SHG. We also try adding SHG or SAM module in the low depth-range DS-SIDENet, the accuracy does not improve much. In addition, we find that it is better to add SAM module as the third decoding block. Adding such module at the fourth or fifth block will not improve the accuracy much, but the efficiency is reduced due to larger feature map size.

5.3.3 Scene understanding stage: scene classification vs. coarse depth estimation

We introduced two scene understanding methods in the robust SIDE, the scene classification, and the coarse depth estimation. The advantage of using scene classification is that it does not depend on actual calculation of depth threshold, so it is more practical in real scenario. But training such network requires collecting various external training data (Places-365 dataset). In contrast, when training the coarse depth estimation, we may use the same training data as the following low depth-range and high depth-range SIDE networks. But setting the threshold σ of depth-range is difficult. The $\sigma = 5.89m$ obtained from ROB validation data can achieve 100% classification accuracy in the ROB testing images, but this is not realistic in real scenario. To evaluate the influence, we further do the following experiments

- R1: Keep the same coarse depth estimation, low depth-range and high depth-range DS-SIDENets trained for the optimal threshold of 5.89m, but change the threshold to 10m

- R2: Keep the same coarse depth estimation and high depth-range DS-SIDENets, but re-train low depth-range DS-SIDENet by mixing all ScanNet images with KITTI images whose maximum depth is lower than 10m. Change the threshold to 10m as well

In Table 9, we give the accuracy of the above two experiments. It can be seen that if the threshold is set to 10m (R1), the KITTI accuracy decreases without re-training low depth-range DS-SIDENet. The reason is that some of

Table 8. Depth estimation accuracy of different high depth-range DS-SIDENets in KITTI validation set, with and w/o SHG/SAM module.

DS-SIDENet	SHG/SAM in decoding	iRMSE	REL
+SHG	Block 3	8.29	0.075
+SAM	Block 3	7.83	0.066
+SAM	Block 4	7.84	0.066
+SAM	Block 5	7.84	0.066
noSHG/SAM	N/A	8.68	0.085

Table 9. Accuracy of different robust SIDE methods in ScanNet test set (RMSE/REL) and KITTI validation set (iRMSE/REL). σ is the threshold to decide the low depth-range and high depth-range. ‘Re-train’ means whether retraining the low depth-range DS-SIDENet by adding the KITTI images with maximum depth lower than σ .

Method	σ	Re-train	ScanNet	KITTI
Ours-sc	N/A	No	0.287/0.138	7.83/0.066
Ours-cde	5.89m	No	0.287/0.138	7.83/0.066
R1	10m	No	0.287/0.138	8.44/0.072
R2	10m	yes	0.366/0.191	8.40/0.071

KITTI images will incorrectly utilize the low depth-range DS-SIDENet for depth estimation. However, the ScanNet accuracy will not change since all ScanNet images are still classified as low depth-range images. If we re-train the low depth-range DS-SIDENet by adding some of KITTI training data (R2), although the KITTI accuracy improves, but the ScanNet accuracy decreases. The reason is that the outdoor context brought by KITTI images is totally different from the indoor context of ScanNet images. As a result, the convergence of the re-trained low depth-range DS-SIDENet will be influenced. This tells us that using coarse depth estimation for scene understanding in robust SIDE (‘ours-cde’) is sensitive to the threshold. In contrast, the one based on scene classification (‘ours-sc’) has better generalization ability in real scenario.

6. Conclusion

In this paper, we proposed a two-stage framework for robust single image depth estimation. A scene understanding module is first applied to categorize the images into low depth-range and high depth-range classes. Different SIDE networks trained specifically for these depth-ranges are utilized to obtain an accurate depth map. In addition, we developed a single image depth estimation network (DS-SIDENet) having an encoding-decoding architecture. The use of depthwise separable convolution in the encoding part ensures a better efficiency. The multi-task training in the decoding network further improves the accuracy compared to single-task network. We showed that our proposed method achieves competitive performance compared to state-of-the-art algorithms on NYU, ScanNet, and KITTI datasets. We achieved the top rank compared to ROB 2018 submissions.

References

- [1] <http://www.robustvision.net/>.
- [2] Ayan Chakrabarti, Jingyu Shao, and Greg Shakhnarovich. Depth from a single image by harmonizing overcomplete local network predictions. In *Advances in Neural Information Processing Systems*, pages 2658–2666, 2016.
- [3] Jia-Ren Chang and Yong-Sheng Chen. Pyramid stereo matching network. In *Proceedings of the IEEE Conference on Computer Vision and Pattern Recognition*, pages 5410–5418, 2018.
- [4] Weifeng Chen, Zhao Fu, Dawei Yang, and Jia Deng. Single-image depth perception in the wild. In *Advances in Neural Information Processing Systems*, pages 730–738, 2016.
- [5] Xinjing Cheng, Peng Wang, and Ruigang Yang. Depth estimation via affinity learned with convolutional spatial propagation network. In *Proceedings of the European Conference on Computer Vision (ECCV)*, pages 103–119, 2018.
- [6] Angela Dai, Angel X Chang, Manolis Savva, Maciej Halber, Thomas Funkhouser, and Matthias Nießner. Scannet: Richly-annotated 3d reconstructions of indoor scenes. In *Proceedings of the IEEE Conference on Computer Vision and Pattern Recognition*, pages 5828–5839, 2017.
- [7] Xianzhi Du, Mostafa El-Khamy, and Jungwon Lee. Amnet: Deep atrous multiscale stereo disparity estimation networks. *arXiv preprint arXiv:1904.09099*, 2019.
- [8] David Eigen and Rob Fergus. Predicting depth, surface normals and semantic labels with a common multi-scale convolutional architecture. In *Proceedings of the IEEE International Conference on Computer Vision*, pages 2650–2658, 2015.
- [9] David Eigen, Christian Puhrsch, and Rob Fergus. Depth map prediction from a single image using a multi-scale deep network. In *Advances in neural information processing systems*, pages 2366–2374, 2014.
- [10] Huan Fu, Mingming Gong, Chaohui Wang, Kayhan Batmanghelich, and Dacheng Tao. Deep ordinal regression network for monocular depth estimation. In *Proceedings of the IEEE Conference on Computer Vision and Pattern Recognition*, pages 2002–2011, 2018.
- [11] Andreas Geiger, Philip Lenz, Christoph Stiller, and Raquel Urtasun. Vision meets robotics: The kitti dataset. *The International Journal of Robotics Research*, 32(11):1231–1237, 2013.
- [12] Derek Hoiem, Alexei A Efros, and Martial Hebert. Automatic photo pop-up. *ACM transactions on graphics (TOG)*, 24(3):577–584, 2005.
- [13] Kevin Karsch, Ce Liu, and Sing Bing Kang. Depth transfer: Depth extraction from video using non-parametric sampling. *IEEE transactions on pattern analysis and machine intelligence*, 36(11):2144–2158, 2014.
- [14] Alex Kendall, Hayk Martirosyan, Saumitro Dasgupta, Peter Henry, Ryan Kennedy, Abraham Bachrach, and Adam Bry. End-to-end learning of geometry and context for deep stereo regression. *CoRR*, vol. abs/1703.04309, 2017.
- [15] Yevhen Kuznietsov, Jörg Stückler, and Bastian Leibe. Semi-supervised deep learning for monocular depth map prediction. In *Proc. of the IEEE Conference on Computer Vision and Pattern Recognition*, pages 6647–6655, 2017.
- [16] Lubor Ladicky, Jianbo Shi, and Marc Pollefeys. Pulling things out of perspective. In *Proceedings of the IEEE Conference on Computer Vision and Pattern Recognition*, pages 89–96, 2014.
- [17] Iro Laina, Christian Rupprecht, Vasileios Belagiannis, Federico Tombari, and Nassir Navab. Deeper depth prediction with fully convolutional residual networks. In *3D Vision (3DV), 2016 Fourth International Conference on*, pages 239–248. IEEE, 2016.
- [18] Bo Li, Yuchao Dai, and Mingyi He. Monocular depth estimation with hierarchical fusion of dilated cnns and soft-weighted-sum inference. *Pattern Recognition*, 83:328–339, 2018.
- [19] Jun Li, Reinhard Klein, and Angela Yao. A two-streamed network for estimating fine-scaled depth maps from single rgb images. In *Proceedings of the 2017 IEEE International Conference on Computer Vision, Venice, Italy*, pages 22–29, 2017.
- [20] Ruibo Li, Ke Xian, Chunhua Shen, Zhiguo Cao, Hao Lu, and Lingxiao Hang. Deep attention-based classification network for robust depth prediction. *arXiv preprint arXiv:1807.03959*, 2018.
- [21] Fangchang Ma and Sertac Karaman. Sparse-to-dense: depth prediction from sparse depth samples and a single image. *arXiv preprint arXiv:1709.07492*, 2017.
- [22] Haoyu Ren, Mostafa El-Khamy, and Jungwon Lee. Image super resolution based on fusing multiple convolution neural networks. In *CVPRW*, pages 54–61, 2017.
- [23] Haoyu Ren, Mostafa El-Khamy, and Jungwon Lee. Dn-resnet: Efficient deep residual network for image denoising. *ACCV*, 2018.
- [24] Olaf Ronneberger, Philipp Fischer, and Thomas Brox. U-net: Convolutional networks for biomedical image segmentation. In *International Conference on Medical image computing and computer-assisted intervention*, pages 234–241. Springer, 2015.
- [25] Ashutosh Saxena, Sung H Chung, and Andrew Y Ng. 3-d depth reconstruction from a single still image. *International journal of computer vision*, 76(1):53–69, 2008.
- [26] Dan Xu, Elisa Ricci, Wanli Ouyang, Xiaogang Wang, and Nicu Sebe. Multi-scale continuous crfs as sequential deep networks for monocular depth estimation. In *Proceedings of CVPR*, volume 1, 2017.
- [27] Bolei Zhou, Agata Lapedriza, Aditya Khosla, Aude Oliva, and Antonio Torralba. Places: A 10 million image database for scene recognition. *IEEE Transactions on Pattern Analysis and Machine Intelligence*, 2017.